

Increased Energy Absorption into W due to the Metal Deposited Layer from an ELM-like Pulsed Plasma

Takaya NAKAMORI, Noriyasu OHNO, Hirohiko TANAKA, Shin KAJITA¹⁾,
Yusuke KIKUCHI²⁾ and Tsuyoshi AKIYAMA³⁾

Graduate School of Engineering, Nagoya University, Nagoya 464-8603, Japan

¹⁾*Institute of Materials and Systems for Sustainability, Nagoya University, Nagoya 464-8603, Japan*

²⁾*Graduate School of Engineering, University of Hyogo, Himeji 671-2280, Japan*

³⁾*National Institute for Fusion Science, National Institutes of Natural Sciences, Toki 509-5292, Japan*

(Received 28 November 2018 / Accepted 8 February 2019)

It is important in divertor physics research to investigate thermal response process of beryllium deposited tungsten to high transient heat load such as ELMs. We investigated the heat load on aluminum-coated tungsten by comparing the measured back surface temperature and calculation results of the one-dimensional heat conduction equation. When the plasma power was low enough so that the evaporation did not occur sufficiently, the heat load on the aluminum-coated tungsten was higher than the virgin tungsten. It was caused by the reduction in the energy reflection coefficient due to the formation of aluminum layer. The results suggested that the beryllium deposited layer adversely affects the heat load on the divertor plate when the heat load was not high such as Grassy-ELM.

© 2019 The Japan Society of Plasma Science and Nuclear Fusion Research

Keywords: aluminum coating, plasma gun, energy reflection, vapor shielding

DOI: 10.1585/pfr.14.1401051

1. Introduction

In magnetic confinement fusion devices, plasma facing components are exposed to high transient heat load due to the Edge Localized Modes (ELMs). Because the heat flux due to the type I ELM to the divertor plate is expected to reach $0.2\text{--}2\text{ MJ/m}^2$ [1], there is a concern that serious damage could occur on the divertor plate. In order to estimate the lifetime of the divertor plate, it is indispensable to understand the thermal response process against the huge transient heat load on divertor plate.

From past researches, it is known that material damages such as cracking, melting, droplet, and evaporation are caused due to the transient heat load. Here, the vapor cloud generated from the deposited materials on the tungsten (W) surface (e.g., beryllium (Be) sputtered from the first wall [2]) is considered to reduce subsequent heat loads; the phenomenon is called vapor shielding effect. Vapor generation and reduction of the electron temperature near the Be target were confirmed in PISCES-B experiments and particle-in-cell simulations [3]. The vapor shielding effect was also investigated using the plasma gun devices that can simulate ELM events [4, 5]. On the other hand, considering the energy reflection on the material surface, the low-Z materials like Be could easily transfer the plasma energy to the material compared with the high-Z material, because mass ratios of the low-Z material to the main plasma species such as hydrogen isotopes and helium (He) are closer to unity. Therefore, it is important to study

about the energy reflection in addition to the vapor shielding effect.

In this study, we performed evaluations of energy inflows on W plates with/without deposited layers from the pulsed plasma in NAGDIS-PG (NAGoya DIvertor Simulator - with Plasma Gun). Since Be is known to be toxic material, we used aluminum (Al) as a proxy material and investigated how the Al deposited layer affects the heat load on W. In order to estimate the heat load on the Al surface, we measured the back surface temperature of the sample with high temporal resolution ($\sim 10\text{ }\mu\text{s}$), and, then, one-dimensional (1D) heat conduction equation was numerically calculated.

In the following section, setups of the experiment and the 1D heat calculation will be described. In Sec. 3, heat load evaluations on different-thickness samples will be shown. Obtained results will be compared with the other plasma gun study in Sec. 3.4. Finally, this study will be summarized in Sec. 4.

2. Setup

2.1 Plasma gun and the measurement system

We used the NAGDIS-PG as a pulsed plasma irradiation device [6]. NAGDIS-PG is composed of the steady state plasma generator NAGDIS-I and the pulsed plasma generator MCPG (Magnetized Coaxial Plasma Gun), as shown in Fig. 1. In this study, we irradiated only with the pulsed plasma without the steady state plasma. Typical

author's e-mail: nakamori-takaya@ees.nagoya-u.ac.jp

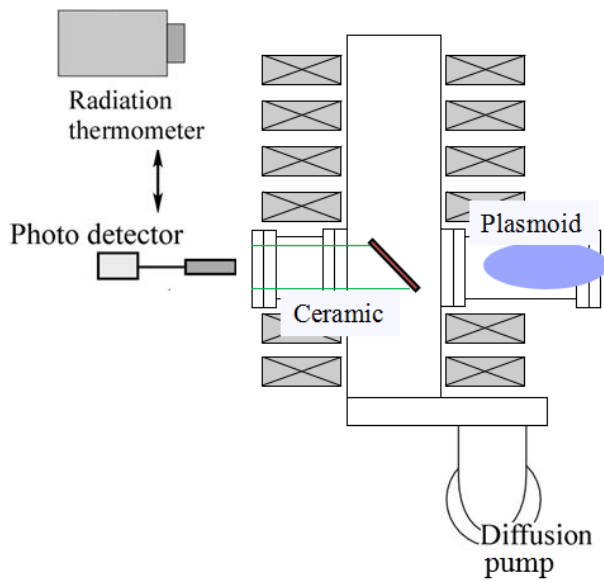


Fig. 1 Schematic of setup at NAGDIS-PG.

ion temperature and electron density of a pulsed plasma are ~ 20 eV and $\sim 10^{21} - 10^{22} \text{ m}^{-3}$, respectively. We used He as the discharge gas. A bulk pristine W sample and three W samples with different thin Al layer coated with the magnetron sputtering device were used. The size of the W samples was $50 \times 60 \times 0.1$ mm and the thickness of the Al coating was 1, 3 and 8 μm . These samples were placed at an angle of 45 degrees to the direction of the pulsed plasma injection.

Heat load absorbed on the sample was estimated by comparing the sample temperature and calculation results of the 1D heat conduction equation. The sample temperature was measured by measuring the infrared radiation from the back surface of the sample using an indium gallium arsenide (InGaAs) photo detector. In order to eliminate the light emission from the pulsed plasma, a ceramic tube was inserted between the sample and the viewing window without any aperture inside the vacuum vessel [7]. We calibrated the output of photo detector by a radiation thermometer. Figure 2 shows typical temporal evolutions of the MCPG discharge current I_{gun} and the back surface temperature. It can be found that temperatures higher than ~ 700 K could be measured with small perturbation.

2.2 Heat load calculation with 1D conduction equation

After the measurements of the back surface temperature, absorbed heat load on the sample was estimated with the help of 1D heat conduction equation calculation [7]. We prepared a calculation model consisting of two layers of Al and W for calculating the heat conduction in thin Al and thick W. In this model, after the calculation of the thin Al region with shorter time step, the calculation of the W region with longer time step was performed. The grid of

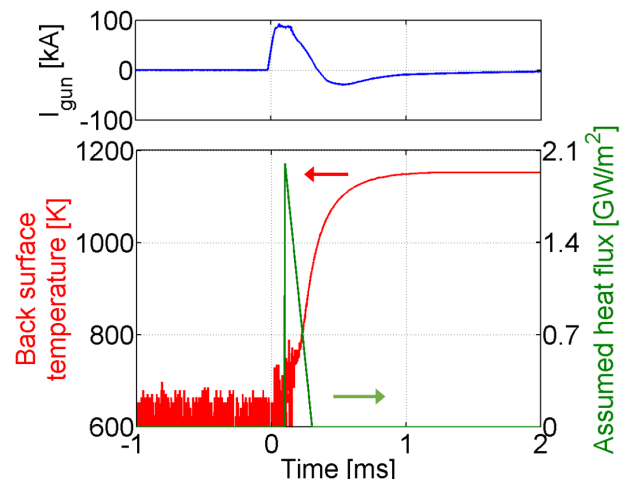


Fig. 2 Typical time evolution of discharge current I_{gun} (blue line) and the back surface temperature of W sample (red line), assumed heat flux in 1D heat conduction equation (green line).

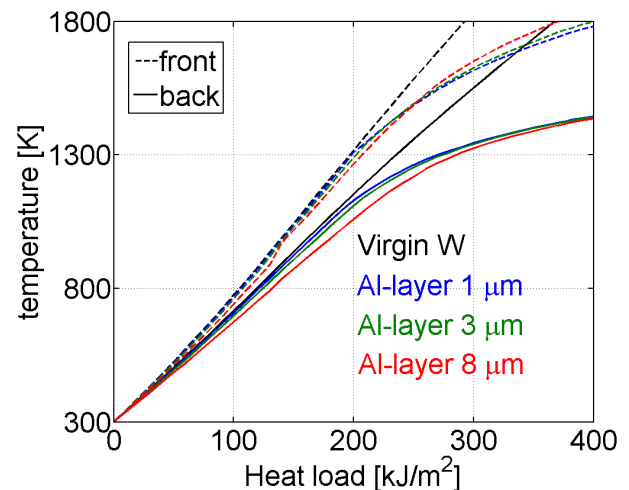


Fig. 3 Heat load vs. maximum sample temperature in the 1D heat conduction calculation.

the Al and W region were connected with using the same temperature and heat flow (temperature gradient). At the front surface, we considered the input heat load and the radiation. At the back surface, the radiation was only considered. Shape of the input heat load was assumed to be the sawtooth waveform as shown in Fig. 2. Thermal properties of materials were used by AIST database [8]. In this study, the latent heat was not taken into consideration, because it was much smaller than pulsed plasma heat load. Figure 3 shows the relationship between the heat load and the maximum temperature of the sample calculated using the 1D heat conduction equation model. It is mentioned in Fig. 3 that the Al layer thickness does not significantly affect the relationship between the surface temperature and the incoming heat load. In case of Al-coated W, when

the surface temperature becomes over the Al melting point (933 K), thermal conductivity, specific heat capacity, and density of Al change greatly, thus the gradient of the temperature with respect to the heat load becomes small.

3. Result

3.1 Back surface temperature measurement and absorbed heat load calculation

Figure 4 shows the maximum temperature and the heat load as a function of the thickness of the Al layer. Ten pulsed plasmas were irradiated to each sample. The mean and standard deviation were plotted with the symbol and the error bar, respectively. The back surface temperature reached ~ 1250 K with the heat load of ~ 260 kJ/m^2 when the Al-layer thickness was $8 \mu\text{m}$. The maximum temperature increased with the deposition layer thickness from 1100 to 1250 K. The calculated heat load on W with 3 and $8 \mu\text{m}$ Al layers were larger than virgin W and W with $1 \mu\text{m}$ Al layer. The mechanism of this increase will be discussed later.

3.2 Consideration with the energy reflection coefficient

One of the possibility to increase the absorbed heat load on the Al-coated W was in the variation of energy reflection coefficient after the Al deposition, because W and Al should have different energy reflection coefficient. Energy reflection coefficient is determined by the incident atomic species, target atom species, incident ion energy (E_i), and angle of incident.

Table 1 shows the energy reflection coefficient of He with respect to Al, W, Be, and iron (Fe) at $E_i = 20$, 50 and 100 eV in the case of normal incident from NIFS database [9]. Energy reflection coefficient becomes high when Z is large and E_i is small. We calculated the heat flux to Al (q_{Al}) and W (q_{W}) surfaces using the ion and electron heat flux written as

$$q_i = n_{\text{se}} C_s \{ (1 - R_{\text{ie}}) [2k_{\text{B}} T_i - e(\varphi_{\text{pw}} - \varphi_{\text{ps}})] + e\varphi_r \}, \quad (1)$$

$$q_e = 2k_{\text{B}} T_e \frac{1}{4} n_{\text{se}} \bar{C}_e \exp \left[\frac{e(\varphi_{\text{pw}} - \varphi_{\text{ps}})}{k_{\text{B}} T_e} \right], \quad (2)$$

where n_{se} , C_s , R_{ie} , k_{B} , φ_{pw} , φ_{ps} , φ_r , and C_e are the electron density at sheath edge, ion sound velocity, energy reflection coefficient, Boltzmann constant, potential difference between plasma and a wall surface, potential difference between plasma and a sheath edge, surface recombination energy (in He, $\varphi_r = 24.59$ eV), and electron mean thermal velocity, respectively [10]. Considering the past research [11], it was assumed that the $n_{\text{se}} = 1 \times 10^{21} \text{ m}^{-3}$, $T_e = T_i = 20$ eV and potential at solid surface is floating potential. Floating potential calculated by

$$V_f = \frac{T_e}{2} \ln \left\{ 2\pi \frac{m_e}{m_i} \left(1 + \frac{T_i}{T_e} \right) \right\}, \quad (3)$$

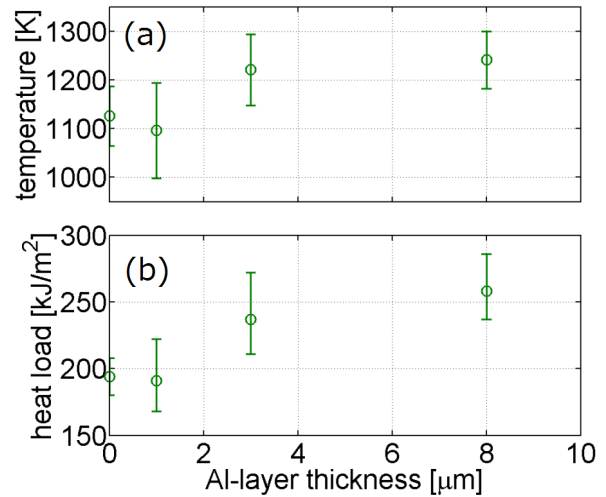


Fig. 4 (a) The highest reached temperature of the back surface and (b) inflow heat load as a function of Al-layer thickness.

Table 1 Energy reflection coefficient of He with respect to W, Fe, Al and Be.

E_i [eV]	W	Fe	Al	Be
Z	74	26	13	4
20	0.528	-	0.215	0.037
50	0.452	0.292	0.145	0.022
100	0.407	0.245	0.121	0.016

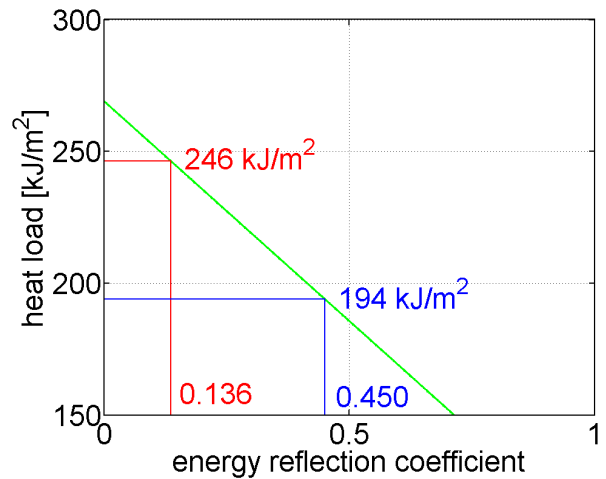


Fig. 5 Effective inflow heat load vs. energy reflection coefficient.

was -63.7 V. The energy reflection coefficient at $E_i = 63.7$ eV was calculated to be 0.136 for Al, 0.450 for W and 0.274 for Fe by spline interpolation. As a result of calculation, q_{Al} is 1.27 times larger than q_{W} . Figure 5 shows the relationship between the absorbed heat load and the energy

Table 2 Surface composition analysis result of EDS.

target	Al 1 μm (before)		Al 1 μm (after)		Al 3 μm (after)		Al 8 μm (after)	
	weight%	atomic%	weight%	atomic%	weight%	atomic%	weight%	atomic%
O	2.85	4.71	17.19	44.57	9.41	24.34	8.77	21.39
Al	97.15	95.29	3.01	4.43	6.60	10.13	35.93	51.96
S					6.68	8.62		
Fe			61.69	43.84	66.50	49.29	30.64	21.41
Ni					10.82	7.63		
Mo			17.32	7.17				
W							24.66	5.24

reflection coefficient when $q_w = 194 \text{ kJ/m}^2$, which was obtained in Fig. 4. From this relation, q_{Al} is estimated to be 246 kJ/m^2 analytically (see Fig. 5). This value coincides with the heat load when the Al deposited layer was 3 and 8 μm . However, when the Al deposited layer was 1 μm , the experimental result was lower than the estimated q_{Al} .

3.3 Investigation of sample surface condition

In the previous subsection, by considering the energy reflection coefficient, the heat loads on W with thin Al layers were lower than the estimated of q_{Al} . To understand the mechanism to cause the discrepancy on thin Al sample, we investigated the sample surface condition by scanning electron microscope (SEM) and energy dispersive x-ray spectroscopy (EDS).

Figure 6 shows SEM images before and after the pulsed plasma irradiations. Cracking and melting are seen on the irradiated Al-coated W. Table 2 shows the EDS result, where S, Ni, and Mo are sulfur, nickel, and molybdenum, respectively. Since the tungsten as the substrate was not detected with a thickness of 1 μm , it is considered that the surface of the Al layer was observed. Composition ratios of Fe and oxygen (O) increased after the irradiation of 10 pulses. Interfusion of O seems to be attributed to the atmosphere exposure after plasma irradiation. Similar to a previous study [6], Fe would be ejected from the electrode of plasma gun and/or vacuum vessel and might be deposited on the material surface. In the case of 8 μm , composition ratio of Al is higher than that of Fe. On the other hand, in the case of 1 and 3 μm , Fe becomes dominant. Because R_{ie} with respect to Fe is higher than that of Al (see Table 1), R_{ie} with respect to the Fe-mixed Al layer would be higher than that of Al. Therefore, the estimated heat load of 246 kJ/m^2 in Fig. 5, where the pure Al layer was assumed, would be overestimated when the Al layer thickness is 1 and 3 μm . Supposing that equal amounts of Al and Fe were deposited on the surface and the effective energy reflection coefficient was 0.205 (inter-

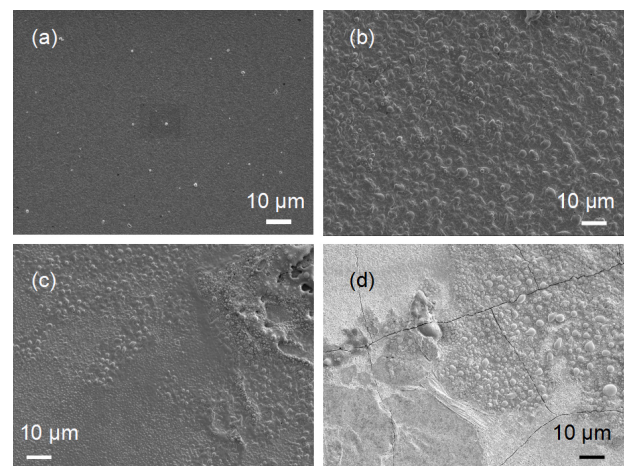


Fig. 6 SEM images of Al-coated W sample surfaces (a) before, and after 10 shots with the Al-layer thicknesses of (b) 1 μm , (c) 3 μm , and (d) 8 μm .

mediate between Al and Fe), the inflow heat load could be estimated to 234 kJ/m^2 , which is close to the experimental results when the Al layer thickness is 1 and 3 μm .

3.4 Comparison with the previous research

Our result shows that the Al-coating increases the heat load to W. Contrary to our results, a previous study reported the Al-coating decreased the heat load [12]. Here we have to take into consideration of the irradiation conditions. In the previous study, it is considered that the surface temperature, inflow heat load, and evaporative Al flux were $\sim 1800 - 2700 \text{ K}$, $\sim 600 \text{ kJ/m}^2$, and $\sim 10^{24-27} \text{ atoms/m}^2\text{s}$ (see Fig. 7 [13]), respectively. In contrast in this study, they were $\sim 1500 \text{ K}$, $\sim 200 \text{ kJ/m}^2$, and $\sim 10^{22} \text{ atoms/m}^2\text{s}$. Because evaporative flux in this study was approximately 10^{2-5} times smaller than that of previous study, the influence of vapor shielding effect seemed to be negligible. It was likely that the influence from the variation of the energy reflection was greater than that of the vapor shielding.

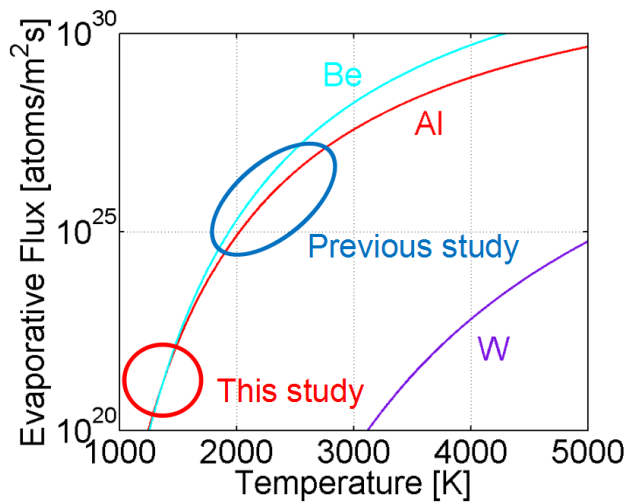


Fig. 7 Temperature dependence of evaporative flux.

4. Summary

We investigated the influence of Al deposited layer on pulsed plasma heat load using the NAGDIS-PG. Absorbed heat load increased when an Al layer was deposited on W sample compared with virgin W sample without Al deposition. This was probably caused by the fact that the energy reflection coefficient of Al is lower than that of W.

In the comparison with the previous study, it was suggested that the heat load to W might be increased by the

Al-coating due to the difference of energy reflection coefficient when the heat load is small and vapor shielding is not noticeable.

For the small-amplitude ELMs such as Grassy-ELMs and type III-ELMs, an increase in the energy deposition on the Be-coated divertor could occur as same as the present study.

Acknowledgments

This work was supported by the NINS program of Promoting Research by Networking among Institutions (Grant Number 01411702).

- [1] G. Federici *et al.*, Plasma Phys. Control. Fusion **45**, 1523 (2003).
- [2] S. Brezinsek *et al.*, Nucl. Fusion **55**, 063021 (2015).
- [3] K. Ibanez *et al.*, Nucl. Mater. Energy **12**, 278 (2017).
- [4] I. Sakuma *et al.*, J. Nucl. Mater. **463**, 233 (2015).
- [5] Y. Kikuchi *et al.*, Phys. Scr. **T167**, 014065 (2016).
- [6] S. Kajita *et al.*, J. Nucl. Mater. **438**, S707 (2013).
- [7] D. Sato *et al.*, Nucl. Fusion **57**, 066028 (2017).
- [8] AIST, “Network Database System for Thermophysical Property Data”, <https://tpds.db.aist.go.jp/>
- [9] W. Eckstein, “Calculated Sputtering, Reflection and Range Values”, IPP-Report 9/132 (2002).
- [10] S. Masuzaki *et al.*, J. Nucl. Mater. **223**, 286 (1995).
- [11] S. Kajita *et al.*, J. Appl. Phys. **51**, 01AJ03 (2012).
- [12] K. Ibanez *et al.*, Contrib. Plasma Phys. **58**, 594 (2018).
- [13] D.E Gray, American Institute of Physics Handbook 3rd edn., New York: McGraw-Hill (1972) pp.4-315.